

ONSET OF DECONFINEMENT IN Pb+Pb COLLISIONS AT THE CERN SPS*

P. SEYBOTH^m, C. ALTⁱ, T. ANTICIC^y, B. BAATAR^h, D. BARNA^d, J. BARTKE^f
 L. BETEV^j, H. BIAŁKOWSKA^u, C. BLUMEⁱ, B. BOIMSKA^u, M. BOTJE^a, J. BRACINIK^c
 R. BRAMMⁱ, P. BUNČIĆ^j, V. CERNY^c, P. CHRISTAKOGLU^b, P. CHUNG^t
 O. CHVALAⁿ, J.G. CRAMER^p, P. CSATÓ^d, P. DINKELAKERⁱ, V. ECKARDT^m
 D. FLIERLⁱ, Z. FODOR^d, P. FOKA^g, V. FRIESE^g, J. GÁL^d, M. GAŻDZICKI^{9,11}
 V. GENCHEV^s, G. GEORGIOPOULOS^b, E. GŁADYSZ^f, K. GREBIESZKOW^v, S. HEGYI^d
 C. HÖHNE^g, K. KADIJA^y, A. KAREV^m, D. KIKOLA^w, M. KLIEMANTⁱ, S. KNIEGEⁱ
 V.I. KOLESNIKOV^h, E. KORNAS^f, R. KORUS^k, M. KOWALSKI^f, I. KRAUS^g
 M. KREPS^c, A. LASZLO^d, R. LACEY^t, M. VAN LEEUWEN^a, P. LÉVAI^d, L. LITOV^r
 B. LUNGWITZ^j, M. MAKARIEV^r, A.I. MALAKHOV^h, M. MATEEV^r, G.L. MELKUMOV^h
 A. MISCHKE^a, M. MITROVSKIⁱ, J. MOLNÁR^d, ST. MRÓWCZYŃSKI^k, V. NICOLIC^y
 G. PÁLLA^d, A.D. PANAGIOTOU^b, D. PANAYOTOV^r, A. PETRIDIS^b, W. PERYT^w
 M. PIKNA^c, J. PLUTA^w, D. PRINDLE^p, F. PÜHLHOFERⁱ, R. RENFORDTⁱ, C. ROLAND^e
 G. ROLAND^e, M. RYBCZYŃSKI^k, A. RYBICKI^{f,j}, A. SANDOVAL^g, N. SCHMITZ^m
 T. SCHUSTERⁱ, F. SIKLÉR^d, B. SITAR^c, E. SKRZYPCZAK^v, M. SŁODKOWSKI^w
 G. STEFANEK^k, R. STOCKⁱ, C. STRABELⁱ, H. STRÖBELEⁱ, T. SUSÁ^y
 I. SZENTPÉTERY^d, J. SZIKLAI^d, M. SZUBA^w, P. SZYMANSKI^{10,20}, V. TRUBNIKOV^u
 D. VARGA^{4,10}, M. VASSILIOU^b, G.I. VERES^{4,5}, G. VESZTERGOMBI^d, D. VRANIĆ^g
 A. WETZLERⁱ, Z. WŁODARCZYK^k, I.K. YOO^o, J. ZIMÁNYI^d

^aNIKHEF, Amsterdam, The Netherlands

^bDepartment of Physics, University of Athens, Athens, Greece

^cComenius University, Bratislava, Slovakia

^dKFKI Research Institute for Particle and Nuclear Physics, Budapest, Hungary

^eMIT, Cambridge, USA

^fInstitute of Nuclear Physics, Cracow, Poland

^gGesellschaft für Schwerionenforschung (GSI), Darmstadt, Germany

^hJoint Institute for Nuclear Research, Dubna, Russia

ⁱFachbereich Physik der Universität, Frankfurt, Germany

^jCERN, Geneva, Switzerland

^kInstitute of Physics Świętokrzyska Academy, Kielce, Poland

^lFachbereich Physik der Universität, Marburg, Germany

^mMax-Planck-Institut für Physik, Munich, Germany

ⁿInst. of Particle and Nuclear Physics, Charles Univ., Prague, Czech Republic

^oDepartment of Physics, Pusan National University, Pusan, Republic of Korea

^pNuclear Physics Laboratory, University of Washington, Seattle, WA, USA

^rAtomic Physics Department, Sofia Univ. St. Kliment Ohridski, Sofia, Bulgaria

^sInstitute for Nuclear Research and Nuclear Energy, Sofia, Bulgaria

^tDepartment of Chemistry, Stony Brook Univ. (SUNYSB), Stony Brook, USA

^uInstitute for Nuclear Studies, Warsaw, Poland

^vInstitute for Experimental Physics, University of Warsaw, Warsaw, Poland

^wFaculty of Physics, Warsaw University of Technology, Warsaw, Poland

^yRudjer Boskovic Institute, Zagreb, Croatia

(Received October 3, 2006)

* Presented at the XLVI Cracow School of Theoretical Physics, Zakopane, Poland
May 27–June 5, 2006.

The NA49 fixed-target experiment studied high energy-density matter produced in nucleus–nucleus reactions at the CERN SPS. In central Pb+Pb collisions at 158A GeV the energy density at the early stage substantially exceeds the threshold for quark deconfinement predicted by lattice QCD. The produced matter shows strong transverse and longitudinal flow. Ratios of yields of produced particles are approximately consistent with statistical equilibration. An energy scan through the SPS range revealed structure in the energy dependence of π and K yields as well as of the inverse slopes of transverse mass distributions. These features suggest that a deconfined phase starts to be produced at around 30A GeV in central Pb+Pb collisions. The analysis of fluctuations and correlations has not yet provided evidence for the predicted critical point of QCD.

PACS numbers: 25.75.-q, 25.75.Dw, 25.75.Gz, 25.75.Ld

1. Introduction

Qualitative considerations based on the finite size of hadrons [1] as well as quantum chromodynamics (QCD) calculations on the lattice [2,3] predict that at sufficiently high energy density strongly interacting matter will transform into a state of quasi-free quarks and gluons, the quark gluon plasma (QGP). Theoretical investigations also found [4] that this phase transition is of first order for finite quark masses and large non-zero baryon density. The phase boundary is predicted to end in a critical point and turn into a rapid crossover as the net baryon density decreases.

The initial stage of high energy collisions of large nuclei provides the best environment to produce the deconfined phase of matter in the laboratory [5,6]. Lead ions first became available at the CERN SPS in 1994. In the first publication from this programme [7] NA49 demonstrated that in central Pb+Pb collisions at top SPS energy the initial energy density exceeds the critical value of $\approx 1 \text{ GeV/fm}^3$. The SPS experiments found that the reactions produced an explosively expanding fireball. Moreover, originally proposed signatures of the QGP, *i.e.* J/Ψ suppression, strangeness enhancement, and possibly thermal photons and dileptons were observed [8]. However, these signatures are not specific for deconfinement. The NA49 Collaboration, therefore, performed an energy scan from 20–158A GeV in order to search for structure in the energy dependence of hadron production characteristics which could indicate the onset of deconfinement [9]. The measurements indeed suggest structure around 30A GeV [10] which will be discussed below. NA49 also searched for fluctuations which might occur if distinct phases coexisted in the early stage of the reactions or if hadrons froze out close to the critical point estimated [3] to lie in a region accessible at the SPS.

2. Experiment NA49 at the CERN SPS

The main features of the NA49 experiment [11] located in the H2 beam line of the North Experimental Hall (see Fig. 1) are large acceptance precision tracking ($\Delta p/p^2 \approx (0.3-7) 10^{-4} (\text{GeV}/c)^{-1}$) and particle identification in the central and forwards rapidity regions using time projection chambers (TPCs). Charged particles (π, K, p, \bar{p}) are identified mostly from the measurement of their energy loss in the TPC gas (accuracy 3–6%). Yields are obtained by fitting a sum of Gaussian functions for the various particle species to the dE/dx distributions in small bins of momentum p and transverse momentum p_T . At central rapidity the identification is further improved by measurement of the time-of-flight (resolution 60 ps) to arrays of scintillation counter tiles. Strange particles ($K_s^0, \Lambda, \Xi, \Omega$) are detected via decay topology and invariant mass measurement. A forward calorimeter measures the energy of the projectile spectators from which the impact parameter in $A + A$ collisions and the number of participating nucleons are deduced. Also reactions of C and Si ions as well as of deuterons were studied. These beams were produced by fragmentation of the primary Pb beam and selected by magnetic rigidity and by specific energy loss in transmission detectors in the beam line. In addition NA49 pursued an extensive program of proton induced collisions for a study of the evolution of particle production from $p + p$ via $p + \text{Pb}$ to Pb+Pb reactions.

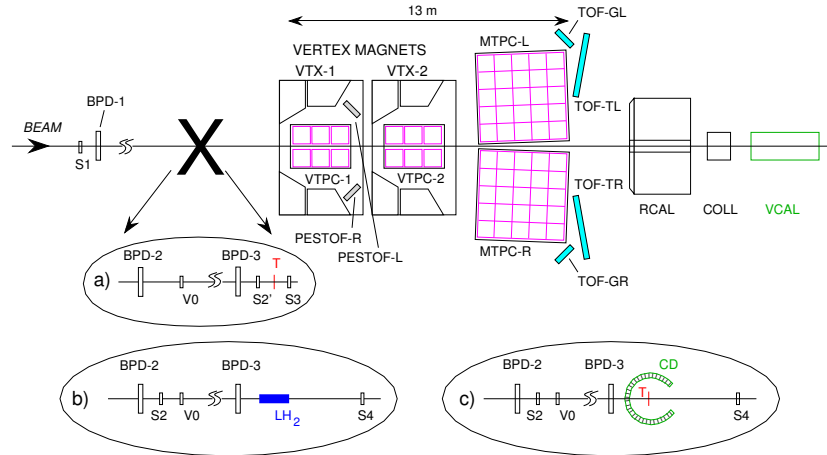


Fig. 1. Schematic layout of the NA49 experiment at the CERN SPS showing beam detectors, superconducting dipole magnets, time projection chambers (VTPC, MTPC), time-of-flight arrays (TOF) and calorimeters (RCAL, VCAL). A thin solid target T is used for $A + A$ collisions (a), which is surrounded by a detector of slow protons (CD) for $p + A$ collisions (c). A liquid H_2 target is employed for $p + p$ collisions (b).

3. Analysis procedure

All events used for physics analysis were required to have a good vertex in the respective target. Tracks of accepted particles had to fulfill quality requirements on the number of measured points and the distance of closest approach to the event vertex. Particle yields have been corrected for acceptance, reconstruction efficiency and feed-down contamination from weak decays. Results on particle yields for the upper 3 energies have been published in [12–14] where more details on the analysis procedures may be found. Results at 20A and 30A GeV are preliminary.

4. Thermal freezeout parameters from spectra and correlations

Midrapidity invariant yields as a function of the transverse mass m_t are shown in Fig. 2 at 20A, 40A and 158A GeV as examples for the large variety of particle species measured by NA49. The spectra become progressively flatter with increasing particle mass, a fact that can be explained by the combined effect of the random thermal momentum distribution and strong radial flow in the produced matter droplet. The development of collective flow is generally attributed to the hydrodynamic pressure generated in the dense early stage [15]. A hydrodynamically based “blast wave” parameterization [16] indeed provides a reasonable description of all the spectra with two parameters: a temperature $T_f \approx (90\text{--}110)\text{ MeV}$ and a radial flow velocity of $\rho_0 \approx 0.8c$ at the surface. These parameters characterize the thermal/kinetic freezeout of the fireball. The pion spectrum overshoots the model curve at low m_t due to the feed-down contribution from resonance decays and this region was, therefore, not used in the fit. More detailed analyses [14, 17] seem to suggest an earlier freezeout of multistrange hyperons at higher temperature and smaller radial flow velocity.

Collective flow also affects quantum statistics induced correlations of identical particles. For negative pion pairs the range of these Bose–Einstein (BE) correlations in momentum difference, which is inversely proportional to the effective pion source size, is reduced by flow. This reduction gets stronger with increasing transverse momentum (see Fig. 3 (left)). In the NA49 publication [18] this effect together with the m_t spectrum of pions was used for the first time to demonstrate strong collective radial flow in Pb+Pb collisions, *i.e.* the correlation of the radial position of the emission points with the transverse momentum of the produced particle. This information cannot be obtained from transverse mass spectra alone. The fitted effective source sizes, the so-called radius parameters R , are shown as a function of averaged transverse momentum k_t of the pion pairs for all the SPS energies in Fig. 3 (right). The decrease of R with increasing k_t due to radial flow is clearly observed. On the other hand, as shown in Fig. 4 (top)

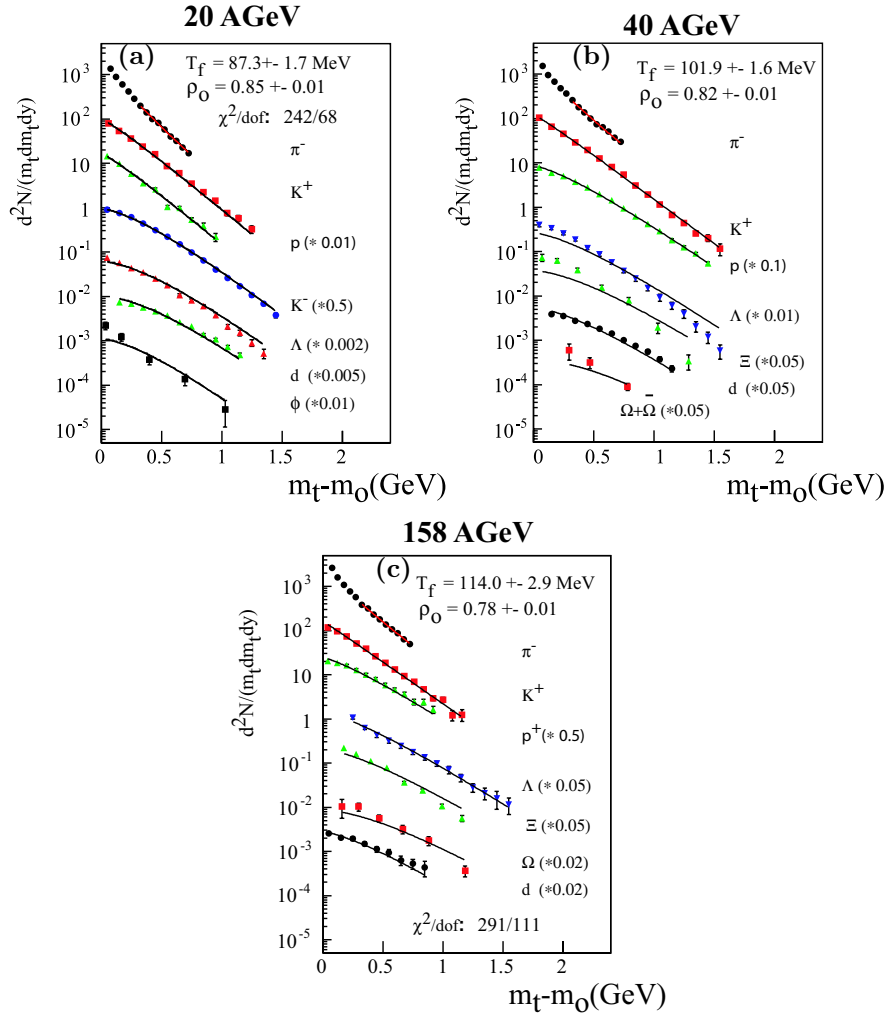


Fig. 2. Transverse mass m_t spectra at midrapidity in central Pb+Pb collisions at 20 A GeV (a), 40 A GeV (b) and 158 A GeV (c). The curves show the result of a blast wave fit [16] with parameters: kinetic freezeout temperature T_f and surface radial flow velocity ρ_0 .

the radius parameters show remarkably little energy dependence over the whole energy range from AGS to RHIC. In particular, there is no indication of an increase of R_{out} at the SPS which might be expected from a first order phase transition. In fact, hydrodynamic calculations with a simple freezeout procedure over-predict the values of R_{out} and R_{long} [15]. A solution of this so-called HBT puzzle seems to lie in a more sophisticated treatment of the freezeout process [19].

The hydrodynamics inspired blast wave parameterization provides a comprehensive description of the kinetic freezeout stage of nucleus–nucleus reactions. The parameterization [16] assumes a uniform pion emission density in a cylinder of radius R and a radial flow velocity increasing linearly with radius to a surface maximum of ρ_0 . Further parameters of the model are the kinetic freezeout temperature T (mainly determined by the m_t spectra), the lifetime τ of the fireball (derived mostly from R_{long}) and the duration $\Delta\tau$ of the pion emission burst (obtained from the difference of R_{out} and R_{side}). Resulting parameter values from simultaneous fits to radii and m_T spectra from AGS to RHIC energies are plotted *versus* collision energy in Fig. 4 (bottom). The corresponding radius parameters at the SPS are shown as curves in Fig. 3 (right). The fit results demonstrate that the matter droplet at freezeout has increased radially by a factor of two and has attained strong

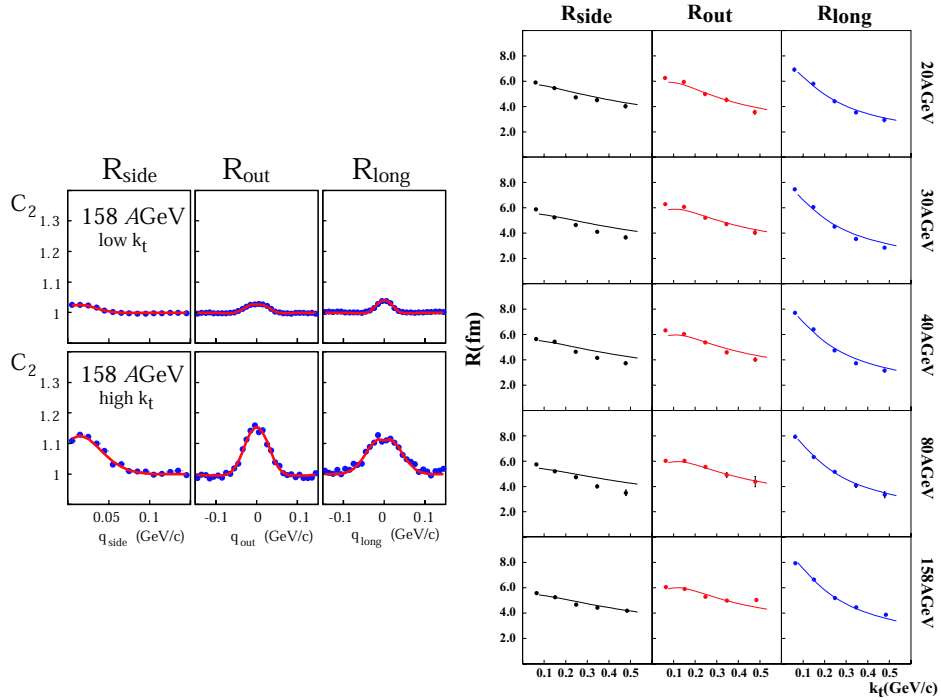


Fig. 3. Left: Projections of the $\pi^-\pi^-$ correlation function on momentum difference q in the transverse (side, out) and beam (long) directions for central Pb+Pb collisions at 158 A GeV. Right: Effective radius parameters R of the pion source *versus* pion pair mean transverse momentum k_t of the pion pairs in central Pb+Pb collisions at the five SPS energies. The curves show results of simultaneous fits of the blast wave model to the radius parameters and the transverse mass m_t spectra of pions and protons. All results refer to midrapidity pion pairs.

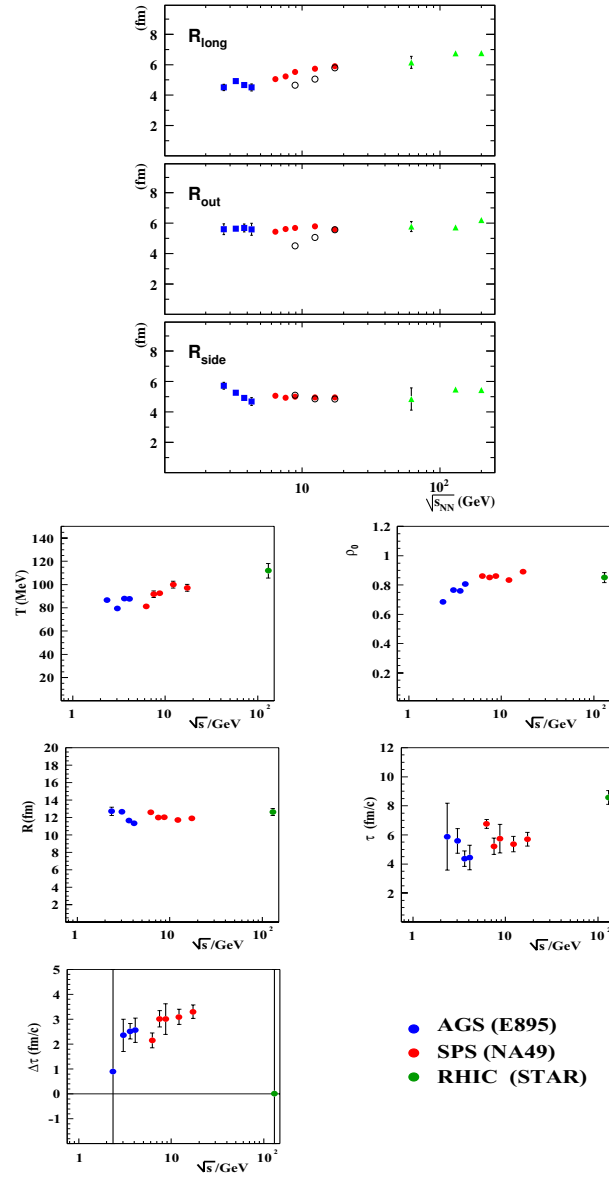


Fig. 4. Top: Energy dependence of radius parameters R of the pion source at mean transverse momentum $k_t = 0.2 \text{ GeV}/c$ and midrapidity in central Pb+Pb and Au+Au collisions. Results from AGS, SPS and RHIC are shown as squares, filled (NA49) and open (NA45) circles, and triangles respectively. Bottom: Freezeout parameters obtained from simultaneous fits of the blast wave model [16] to radius parameters from $\pi^- \pi^-$ Bose-Einstein correlations and m_t spectra of pions and protons at midrapidity in central Pb+Pb (Au+Au) collisions from AGS through SPS (NA49 data) to RHIC energies.

collective radial flow. While freezeout temperature and fireball lifetime appear to increase slowly with energy, the surface radial flow velocity seems to saturate at SPS energies.

While radial flow manifest in m_T spectra and BE correlations builds up over the full lifetime of the fireball, anisotropic flow generated in non-central collisions is particularly sensitive to the properties of the produced matter during the early phase of the reaction. In the almond shaped interaction region anisotropic pressure gradients and rescattering lead to an azimuthally anisotropic momentum distribution. Since the spatial anisotropy disappears quickly, the momentum anisotropy is generated predominantly at early times in the reaction. The pressure rise with initial energy density is qualitatively expected to slow down when deconfinement sets in. Anisotropic flow is quantified by the Fourier expansion coefficients of the azimuthal angular distribution with respect to the reaction plane. At midrapidity the dominant effect is observed in the second coefficient v_2 , termed elliptic flow.

NA49 measured anisotropic flow of pions and protons in Pb+Pb collisions at 40A and 158A GeV [20] and of Λ hyperons [21] at 158A GeV. An example of the Λ azimuthal distribution with respect to the reaction plane as determined from pions is displayed in Fig. 5 (left). The elliptic flow coefficient v_2 at midrapidity is plotted *versus* transverse momentum p_T for the different particle species in Fig. 5 (right).

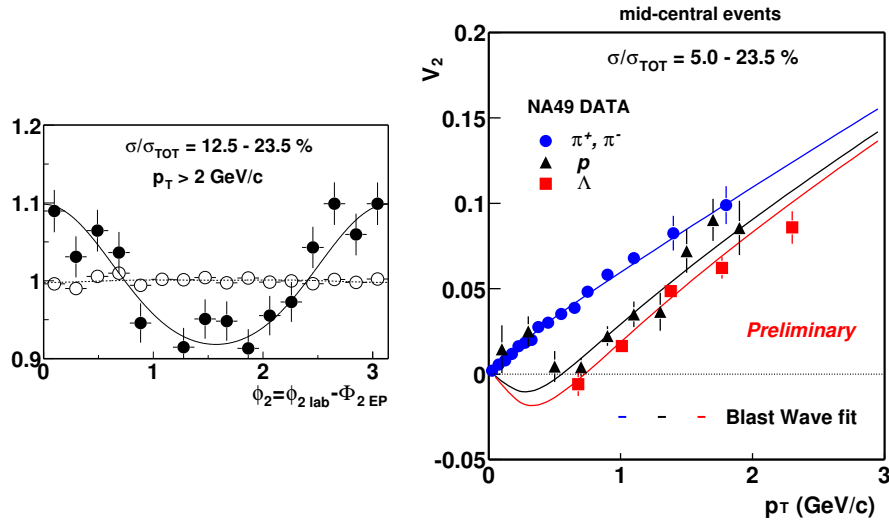


Fig. 5. Left: Azimuthal distribution of Λ hyperons with respect to the reaction plane as determined from pions. Full dots show data, open dots mixed events. Right: v_2 of π, p, Λ versus transverse momentum p_T at midrapidity in Pb+Pb collisions at 158A GeV. Curves show results from the blast wave model [16].

One observes a strong increase with p_T and a clear mass hierarchy as predicted by hydrodynamic models [15]. Values of v_2 are about 30 % higher at RHIC (not shown) than at SPS. Both at the SPS and at RHIC the observed elliptic flow v_2 can be reproduced by the blast wave model parameterization [16] with parameters consistent with those describing spectra and Bose–Einstein correlations [21]. Pure hydrodynamic model calculations over-predict v_2 particularly at SPS energies. However, coupling of a hadronic rescattering phase to the initial deconfined hydrodynamic phase results in reasonable description of the measured energy dependence from SPS to RHIC [22].

5. Hadron freezeout parameters from particle yields

The large acceptance of the NA49 detector allows measurements of rapidity spectra from midrapidity up to almost beam rapidity (see Fig. 6). Rapidity distributions of most particles are peaked at midrapidity. Only Λ

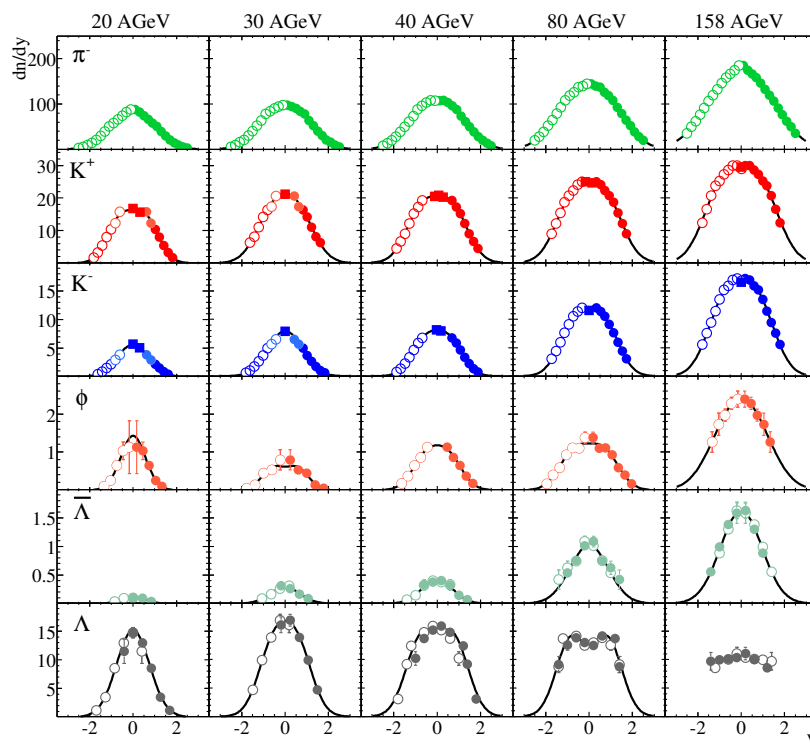


Fig. 6. Rapidity distributions in central Pb+Pb collisions at 20A–158A GeV. Solid dots show measurements, open dots were obtained by reflection around midrapidity.

hyperons, sharing a valence quark with the projectile, show a flattening at higher collision energy. Due to the reflection symmetry of Pb+Pb collisions 4π yields can be determined. Particle yield ratios in $A + A$ (as well as elementary) collisions are consistent with statistical model predictions from threshold to the highest energies using only 3 parameters: a temperature T , a baryo-chemical potential μ_B and a strangeness suppression parameter γ_s . These parameters characterize the freezeout of particle composition after which only the momentum distributions further evolve via elastic scattering. An example of the results of the fit with the statistical model for central Pb+Pb collisions at 158A GeV [23] is shown in Fig. 7 (left).

The resulting parameters T and μ_B [23] are plotted in the phase diagram of hadronic matter in Fig. 7 (right) together with the phase boundary predicted by lattice QCD [3]. One observes that the freezeout points at SPS energies approach the phase boundary and are closest to the critical point at about 60A GeV.

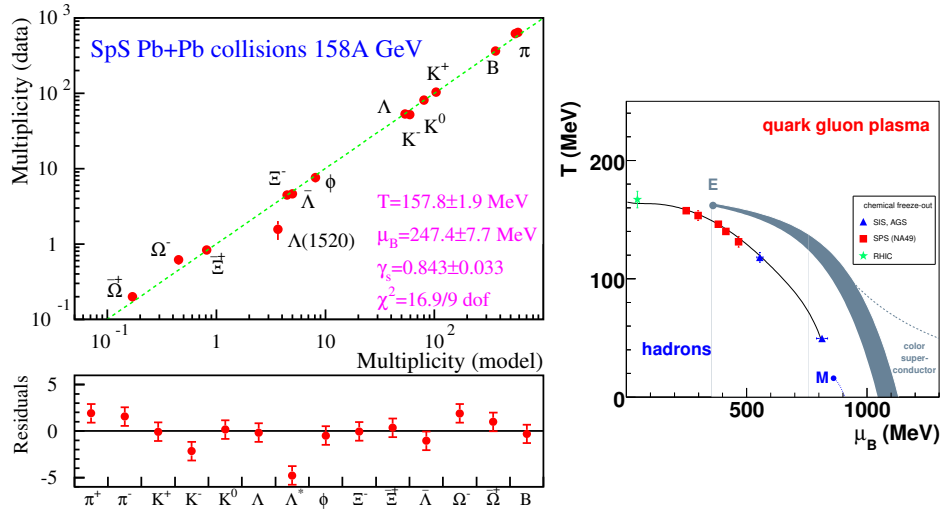


Fig. 7. Left: Results of a statistical model fit to NA49 hadron yields in 158A GeV central Pb + Pb collisions [23]. Right: Phase diagram of hadronic matter showing the hadron composition freezeout points obtained from statistical model fits [23]. The solid curve represents the empirical freezeout condition 1 GeV/hadron [24]. The grey band indicates the expected first order phase boundary between QGP and hadrons which ends in a critical point E estimated from lattice QCD [3].

6. Indications for the onset of deconfinement

A detailed overview of the energy dependence of strangeness production is presented in Fig. 8. The $\langle K^+ \rangle / \langle \pi^+ \rangle$ ratio (a) shows a steep rise from the threshold of kaon production, a maximum around the lowest SPS energy and a decrease to a somewhat lower plateau value. Although the microscopic transport models RQMD, UrQMD [25] and the statistical hadron gas model (full equilibrium version ($\gamma_s = 1$) supplemented by the freezeout condition 1 GeV/hadron [24]) follow the gross trend, they do not reproduce the pronounced peak of the $\langle K^+ \rangle / \langle \pi^+ \rangle$ ratio at the SPS. Since anti-baryon production yields are small, $\langle K^+ \rangle$ counts essentially half of all \bar{s} quarks in the final state (the other half is contained in K^0). In contrast s quarks are distributed between anti-kaons and hyperons (mainly Λ) because of the large net baryon density at SPS energies. As a consequence of the rapid decrease of the net baryon density over the SPS energy range, the sharp

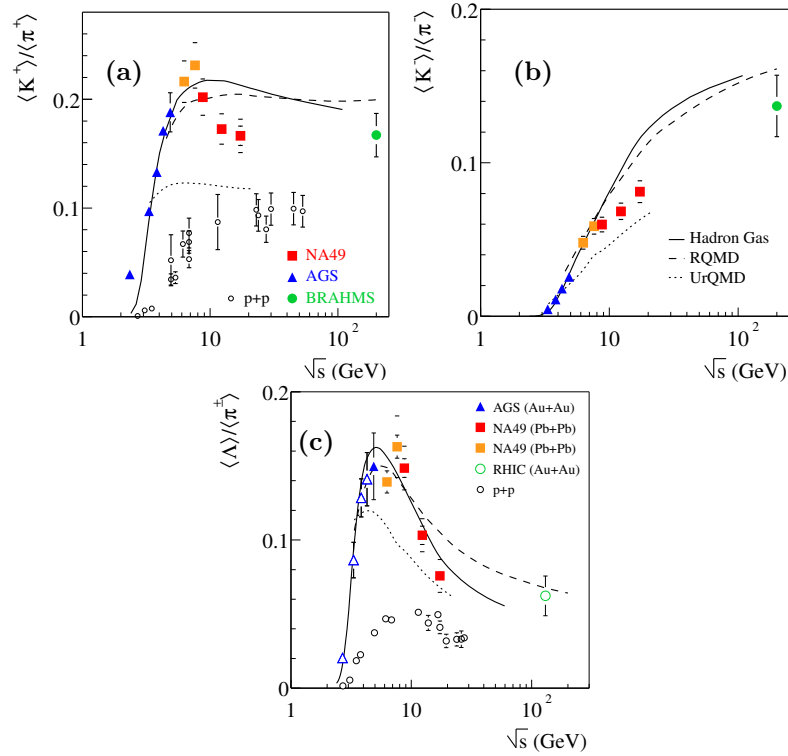


Fig. 8. Ratio of 4 π yields *versus* nucleon–nucleon cms energy \sqrt{s} : $\langle K^+ \rangle / \langle \pi^+ \rangle$ (a); $\langle K^- \rangle / \langle \pi^- \rangle$ (b); $\langle \Lambda \rangle / (0.5(\langle \pi^+ \rangle + \langle \pi^- \rangle))$ (c). Results from $p + p$ collisions (open dots) and model predictions for Pb+Pb collisions (curves) are also shown.

peak in $\langle K^+ \rangle / \langle \pi^+ \rangle$ is reflected in a break in the energy dependence of the $\langle K^- \rangle / \langle \pi^- \rangle$ ratio (Fig. 8 (b)) and a wider maximum in the $\langle \Lambda \rangle / \langle \pi \rangle$ ratio (Fig. 8 (c)).

Using isospin symmetry as well as predictions from the hadron gas model for some unmeasured strange particle species one can obtain an estimate of the number of s and \bar{s} valence quarks contained in the produced particles. The result shown in Fig. 9 (left) demonstrates that there is a break in the energy dependence of total strangeness production at 30A GeV. Dividing by the pion multiplicity (Fig. 9 (right)) confirms the sharp peak already seen in the $\langle K^+ \rangle / \langle \pi^+ \rangle$ ratio. It has been pointed out that these features coincide with a transition from a baryon to a meson dominated final state [26]. However, as seen from the statistical model curve in Fig. 9 (right) this effect cannot adequately describe the measurements.

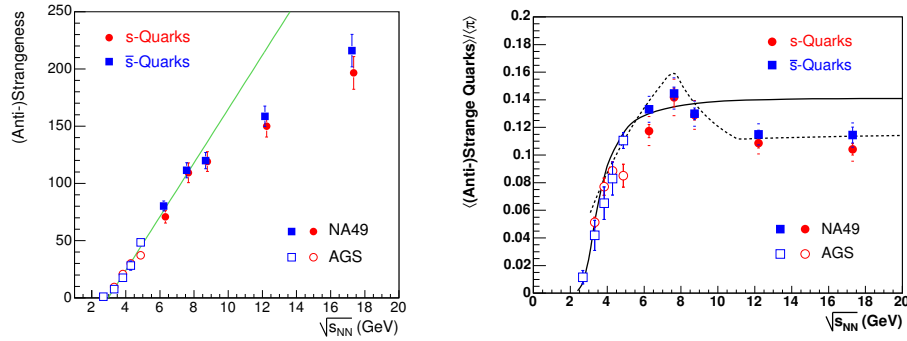


Fig. 9. Left: Estimated multiplicities of all s and \bar{s} valence quarks contained in produced particles as a function of energy. The straight line was obtained from a fit to the low energy points. Right: Ratio of this quantity to the pion multiplicity. The full curve shows the prediction of the statistical model using a parameterization of $\mu_B(\sqrt{s})$ and $\gamma_s = 1$, [24]. The dashed curve depicts the prediction of the SMES model [9].

A close approximation of the total strangeness to pion production ratio can also be calculated from measured yields via the observable $E_S = (\langle K + \bar{K} \rangle + \langle \Lambda \rangle) / \langle \pi \rangle$ which is plotted in Fig. 10 (a) as a function of collision energy. As expected, it shows the same sharp peak followed by a plateau as the $\langle K^+ \rangle / \langle \pi^+ \rangle$ ratio, which is not seen in $p + p$ collisions and not reproduced by hadronic models. On the other hand this feature can be understood in a reaction scenario with the onset of deconfinement around 30A GeV as proposed in the statistical model of the early stage (SMES [9], dash-dotted curve in Fig. 10 (a)). E_S reflects the behavior of the ratio of the number of $s + \bar{s}$ quarks to entropy in the model. It shows a steep threshold rise while the system stays in the hadron phase but drops to the value expected in the QGP at higher collision energies when the fireball initially reaches the

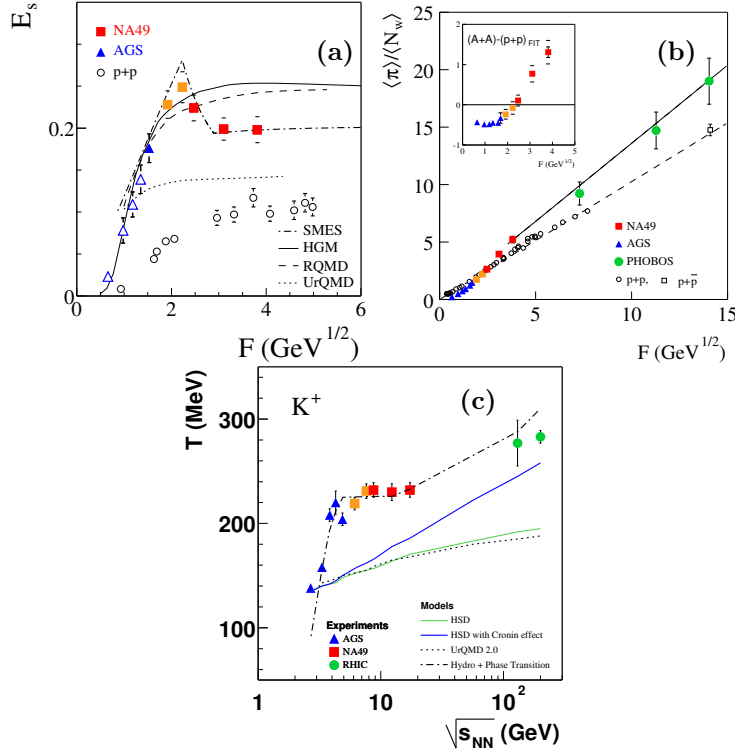


Fig. 10. (a) Relative strangeness yields $E_S = (\langle K + \bar{K} \rangle + \langle \Lambda \rangle) / \langle \pi \rangle$ versus Fermi energy variable $F \approx s_{NN}^{0.25}$. (b) Pion yield per participating nucleon $\langle \pi \rangle / \langle N_w \rangle$ versus F . (c) Energy dependence of the effective temperature parameter T of K^+ transverse mass spectra. Results from $p + p$ collisions are shown as open circles, model predictions for Pb+Pb collisions as curves.

deconfined partonic phase. At the same transition energy of $30A \text{ GeV}$ the rate of increase of the number of produced pions per participating nucleon (a measure of the entropy per baryon in the model) was predicted to increase. As seen in Fig. 10 (b), this seems to be confirmed by the measurements for collisions of heavy nuclei, while there is no change in energy dependence for $p + p$ reactions.

The transverse mass spectrum of kaons is well described by an exponential function $e^{-m_t/T}$. As shown in Fig. 10 (c) for K^+ the inverse slope parameter T rises steeply at low energies, stays at an approximately constant value through the SPS energy range and ends up slightly higher at RHIC energy. Similar behavior is seen for K^- (not shown), but is not observed in $p + p$ collisions. These features have been attributed [27] to the constant pressure and temperature when a mixed phase is present in the early stage of the reaction. In fact, a hydrodynamic calculation [28] model-

ing both the deconfined and the hadronic phases can provide a quantitative description (dash-dotted curve in Fig. 10 (c)). The spectra of other abundantly produced particles are not well fitted by exponential functions (see *e.g.* Fig. 2) but their shape can be characterised by the average value of the transverse mass $\langle m_T \rangle$ minus the rest mass m_0 . The results in Fig. 11 show that the near constancy of the slope of the spectra in the SPS energy range is a common feature for all these particles species.

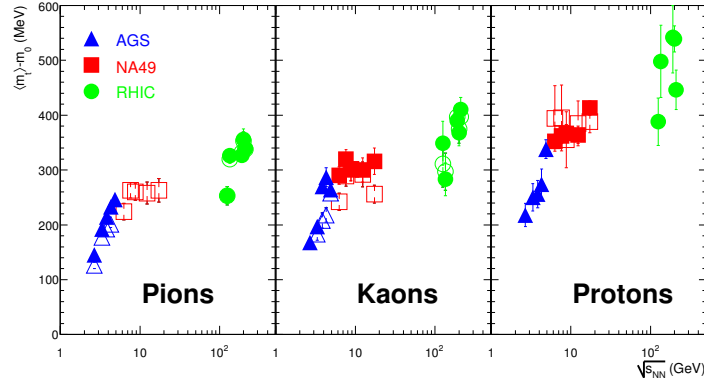


Fig. 11. Energy dependence of $\langle m_T \rangle - m_0$ for π^- and π^+ (left), K^+ and K^- (center), and p and \bar{p} (right) from AGS, SPS and RHIC experiments. Full (open) symbols show results for negatively (positively) charged particles.

7. Results on fluctuations

If the fireball freezeout occurs close to the boundary of a first order phase transition or near the QCD critical point then large event-to-event fluctuations may be expected. The NA49 detector was, therefore, designed with a large acceptance to allow for a wide range of fluctuation and correlation measurements.

The average transverse momentum $\langle p_T \rangle$ in the event is related to the temperature and radial flow in the fireball. The latter might fluctuate with the initial energy density and the fraction of deconfined matter at the early stage of the collision. The distributions for event-wise $\langle p_T \rangle$ are shown in Fig. 12 (left) for central Pb+Pb, Si+Si and $p + p$ collisions at 158A GeV by the data points [29]. These are compared to results from mixed events (histograms) in which correlations are destroyed by construction while preserving the inclusive p_T and multiplicity distributions. Clearly, the fluctuations are close to the statistical limit as represented by the mixed events and no distinct event classes are observed. A quantitative analysis was performed using the quantity Φ_{p_T} which is defined to vanish for purely statistical fluc-

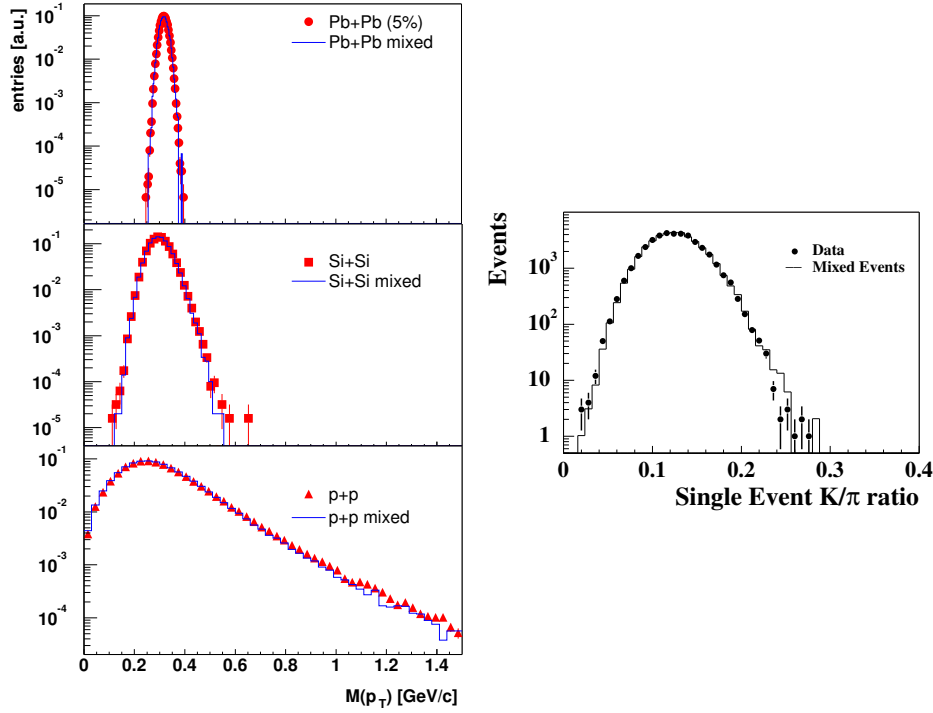


Fig. 12. Left: Distributions of event-wise $\langle p_T \rangle$ in the rapidity interval $1.1 < y < 2.6$ for Pb+Pb, Si+Si and $p+p$ collisions at 158A GeV. Right: Distribution of the event-wise K/π ratio in central Pb+Pb collisions at 158A GeV for laboratory momenta > 3 GeV/c. Results from real events are shown by data points from mixed events by histograms.

tuations and which is furthermore independent of the number of collision participants in superposition models. The results for Φ_{p_T} in the rapidity range $1.1 < y_\pi < 2.6$ are plotted *versus* collision system size in Fig. 13 (left). The measured Φ_{p_T} values are smaller than 5 MeV/c and thus below a few percent of the $\langle p_T \rangle$. Interestingly a significant system size dependence is observed with a maximum for peripheral Pb+Pb collisions. A similar dependence was found for the fluctuations of the multiplicity of negatively charged particles [10]. The two observations may be related due to a possible correlation between $\langle p_T \rangle$ and multiplicity [30].

The energy dependence of the fluctuation measure Φ_{p_T} at the SPS for central Pb+Pb collisions is plotted in Fig. 13 (right). The observed values are small and approximately constant. Somewhat larger results have been obtained near midrapidity by experiment NA45 [31]. At RHIC the $\langle p_T \rangle$ fluctuations increase substantially due to the rise of jet production [32].

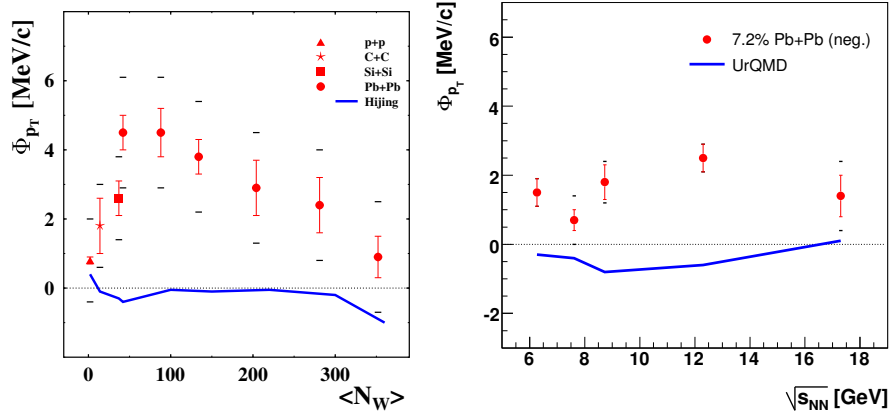


Fig. 13. Left: The $\langle p_T \rangle$ fluctuation measure Φ_{p_T} for negatively charged particles *versus* the number of nucleon participants N_W in $p + p$, $C + C$, $Si + Si$ and $Pb + Pb$ collisions at 158A GeV. The curve shows predictions from the HIJING model filtered through the acceptance of the NA49 detector. Right (preliminary): energy dependence of $\langle p_T \rangle$ fluctuation measure Φ_{p_T} for negatively charged particles in central $Pb + Pb$ collisions. The curve shows predictions from the UrQMD model filtered through the acceptance of the NA49 detector. Results are for the rapidity interval $1.1 < y_\pi < 2.6$.

Fluctuations of the K/π ratio are believed to increase near the critical point. It has also been pointed out [33] that at the onset of deconfinement there could be a significant decrease. The majority of strange quarks in the produced particles are contained in kaons at SPS and RHIC energies. The mass of strangeness carriers in the hadron phase (kaons) is much larger than the temperature whereas in the deconfined phase (strange quarks) it is smaller. Therefore, fluctuations in the initial energy density at fixed collision energy are expected to lead to large fluctuations of the K/π ratio when the system stays in the hadronic phase. However, these K/π ratio fluctuations should significantly decrease if deconfinement occurs during the early stage of fireball evolution [9, 33]. The SMES model curve in Fig. 10 (b) provides an illustration of this generic prediction when one looks at the change of the K/π ratio for small variations of the energy variable F in the respective regions.

The $(K^+ + K^-)/(\pi^+ + \pi^-)$ (as well as $(p + \bar{p})/(\pi^+ + \pi^-)$) ratio was extracted event by event with a maximum likelihood fit method for particles with laboratory momenta larger than 3 GeV/c in central $Pb + Pb$ collisions at the five SPS energies [34]. The momentum cut is necessary to allow identification by specific energy loss of the particles in the TPCs. This leads to acceptances which shift to larger cms rapidities with increasing particle

mass. An example of the distribution of the $(K^+ + K^-)/(\pi^+ + \pi^-)$ ratio at 158A GeV is shown in Fig. 12 (right) where it is also compared to the results from mixed events (histogram) [35]. Clearly, both distributions are very similar and indicate that non-statistical fluctuations are small. Quantitatively, dynamical fluctuations were calculated by comparing the width σ_{data} of the ratio distribution to the one obtained for mixed events from the formula $\sigma_{\text{dyn}}^2 = \sigma_{\text{data}}^2 - \sigma_{\text{mixed}}^2$. As seen from Fig. 14 (left) the dynamical fluctuations of the $(K^+ + K^-)/(\pi^+ + \pi^-)$ ratio amount to only around 5% of the average ratio (about 0.15), but they show a decrease towards higher energy. Preliminary results from the STAR experiment at RHIC for higher energies also indicate values close to those at the highest SPS energy [36]. Such a behaviour is not seen in typical reaction models, *e.g.* UrQMD, but is consistent with the qualitative expectations from the onset of deconfinement [33].

The dynamical fluctuations of the $(p + \bar{p})/(\pi^+ + \pi^-)$ ratio are plotted for the five SPS energies in Fig. 14 (right). The observed negative values are described quantitatively by the UrQMD model and are most likely due to the correlated production of p and π via baryon resonances.

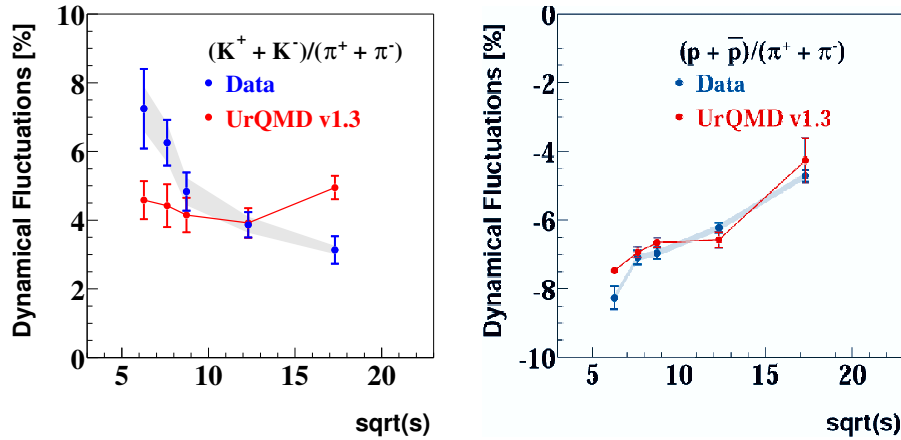


Fig. 14. Energy dependence of dynamical fluctuations of the $(K^+ + K^-)/(\pi^+ + \pi^-)$ ratio (left) and the $(p + \bar{p})/(\pi^+ + \pi^-)$ ratio (right) in central Pb+Pb collisions at the SPS (preliminary).

Electric charge fluctuations were predicted to be strongly reduced if the fireball passed through a QGP phase [37]. Fig. 15 (left) depicts the distribution of net charge in the rapidity range $-1.4 < y < 2.4$ for central Pb+Pb collisions at 158A GeV as an example. As a consequence of charge conservation the data (full histogram) display a narrower distribution than mixed events in which this effect is removed. Fig. 15 (right) shows the mea-

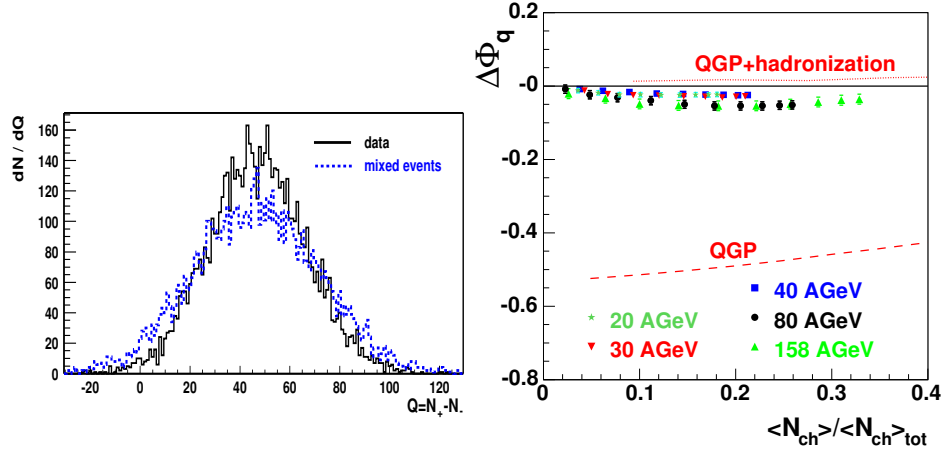


Fig. 15. Left: Distributions of net charge $Q = N^+ - N^-$ for the rapidity range $-1.4 < y < 2.4$ in central Pb+Pb collisions at 158 A GeV for data (full histogram) and mixed events (dotted histogram). Right: Measure $\Delta\Phi_q$ of electric charge fluctuations corrected for charge conservation *versus* rapidity acceptance.

measurements of electric charge fluctuations in terms of the variable $\Delta\Phi_q$ [38] in which effects of global charge conservation are subtracted. Neither significant energy dependence nor the predicted reduction are observed. However, more recent model calculations suggest that hadronisation effects [39] and at SPS also resonance decays [40] probably mask the reduction.

A first order phase transition from the deconfined to the hadronic phase during the early stage of Pb+Pb collisions is expected to result in a softening of the equation of state and consequently in a long lifetime of the mixed phase. The study of the balance function (BF) was suggested as a method to investigate the time of hadron formation [41]. In many models pions are assumed to be created in charge neutral pairs. Due to the buildup of longitudinal flow and rescattering during the evolution of the fireball, the rapidity correlation of opposite charges will be diluted for pairs formed early in the process but will remain narrow for late hadronisation as expected in a mixed phase scenario. This correlation is quantified by the BF which is plotted as a function of the pseudorapidity difference $\Delta\eta$ of the pairs in Fig. 16 (left). The data are compared to shuffled events, in which the pseudo rapidities of the particles are scrambled while the charges are retained. In this way one obtains an estimate of the maximum decorrelation under the condition of charge conservation. It is evident that the data show increasingly shorter range opposite charge correlations beyond the effects of charge conservation as the centrality of Pb+Pb collisions increases.

The widths $\langle\Delta\eta\rangle$ are calculated numerically from the BF distributions and the results are plotted in Fig. 16 (right, top) for the top SPS energy [42] and for RHIC [43]. The width decreases by 17 % and 14 % respectively, for central compared to peripheral collisions for data while it remains constant for shuffled events. Thus the predicted narrowing is observed, although it is now believed that a large part of this effect is due to the increasing strength of radial flow. In fact a model assuming hadron formation by quark coalescence as well as collective radial flow can reproduce the observed width of the BF [44].

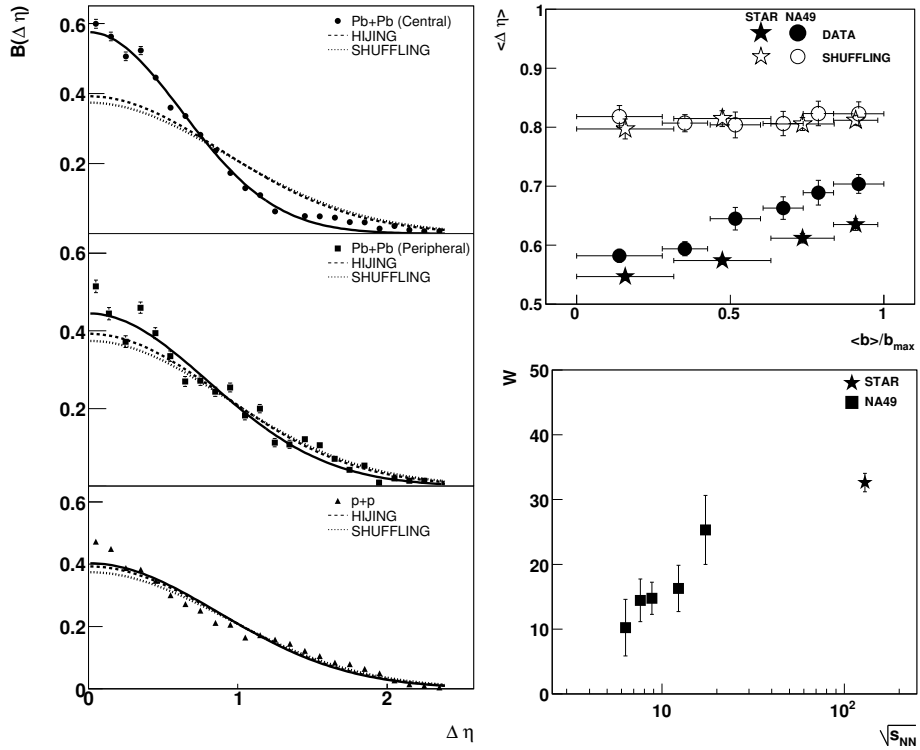


Fig. 16. Left: Balance function *versus* pseudo-rapidity difference of oppositely charged particle pairs at midrapidity and top SPS energy. Curves show Gaussian fits to data (solid), shuffled events (dotted) and HIJING simulation (dashed). Right, top: Width of the balance function *versus* impact parameter at midrapidity in Pb+Pb collisions from NA49 at SPS (dots) and STAR at RHIC (stars). Solid symbols denote data, open symbols show results from shuffled events. Right, bottom: Energy dependence of the normalized narrowing parameter W of the balance function.

In order to be able to compare measurements at different energies and with different acceptance one may calculate the normalized difference (in percent) $W = 100 (\langle \Delta\eta^{\text{shuff}} \rangle - \langle \Delta\eta \rangle) / \langle \Delta\eta^{\text{shuff}} \rangle$ of the widths of the BF for shuffled and real events. The energy dependence of the normalised narrowing parameter W is plotted in Fig. 16 (right, bottom). It shows a steady rise, *i.e.* more narrowing of the BF with respect to uncorrelated particle production throughout the SPS energy range up to RHIC. One does not observe a significant structure at 30A GeV, where other observables suggest the onset of deconfinement.

8. Conclusions

Results from a comprehensive study of nucleus–nucleus collisions in the SPS energy range were presented. The produced matter shows strong transverse and longitudinal flow. Ratios of yields of produced particles are approximately consistent with statistical equilibration. The freezeout parameters of the hadron composition are close to the phase boundary predicted by QCD. The main characteristics of nucleus–nucleus collisions at the highest SPS energy are quite similar to those found at RHIC.

The energy scan of central Pb+Pb collisions revealed that at around 30A GeV the ratio of strangeness to pion production shows a sharp maximum, the rate of increase of the produced pion multiplicity per wounded nucleon increases and the effective temperature of pions and kaons levels to a constant value. These features are not reproduced by present hadronic models but find a natural explanation in a reaction scenario with the onset of deconfinement in the early stage of the reaction at low SPS energy. Further support for this scenario is provided by the decrease of fluctuations of the K/π ratio in the SPS energy range. On the other hand, measurements of fluctuations of the average transverse momentum, of the electric charge, as well as of correlations such as the balance function and $\pi\pi$ Bose–Einstein correlations exhibit a smooth energy dependence.

The present results suggest that further study of the role of the initial volume in the onset of deconfinement and the search for the predicted critical point of QCD are of great interest. This led to an initiative for a low energy program at RHIC [45] and the proposal of a future light-ion program at the SPS [46,47].

My sincere thanks to the organizers of the XLVI School of Theoretical Physics in Zakopane 2006 for supporting my attendance and inviting me to present a review of results from the NA49 experiment. I would also like to express my gratitude to all members of the NA49 Collaboration for their hard and diligent work that produced the comprehensive results presented in this lecture.

REFERENCES

- [1] J. Collins, M. Perry, *Phys. Rev. Lett.* **34**, 1353 (1975).
- [2] F. Karsch, E. Laermann, A. Peikert, *Nucl. Phys.* **B605**, 290 (2002).
- [3] Z. Fodor, S. Katz, *J. High Energy Phys.* **0404**, 50 (2004).
- [4] M. Stephanov, K. Rajagopal, E. Shuryak, *Phys. Rev. Lett.* **81**, 4816 (1998).
- [5] For review of recent results see Proceedings of the 17th International Conference on Ultra-Relativistic Nucleus–Nucleus Collisions, Quark Matter 2004, eds.: H.G. Ritter, X.-N. Wang, *J. Phys. G* **30**, S633 (2004).
- [6] Review of QGP signatures: J. Harris, B. Müller, *Annu. Rev. Nucl. Part. Sci.* **46**, 71 (1996).
- [7] T. Alber *et al.*, *Phys. Rev. Lett.* **75**, 3814 (1995).
- [8] <http://cern.web.cern.ch/CERN/Announcements/2000/NewStateMatter>
- [9] M. Gaździcki, M.I. Gorenstein, *Acta Phys. Pol. B* **30**, 2705 (1999).
- [10] M. Gaździcki (NA49 Collaboration), *J. Phys. G* **30**, S701 (2004).
- [11] S. Afanasiev *et al.*, *Nucl. Instrum. Methods* **A430**, 210 (1999).
- [12] S. Afanasiev *et al.*, *Phys. Rev.* **C66**, 054902 (2002); T. Anticic *et al.*, *Phys. Rev. Lett.* **93**, 022302 (2004); C. Alt *et al.*, *J. Phys. G* **30**, S119 (2004).
- [13] H. Appelshäuser *et al.*, *Phys. Lett.* **B444**, 523 (1998); T. Anticic *et al.*, *Phys. Rev. Lett.* **93**, 022302 (2004).
- [14] C. Alt *et al.*, *Phys. Rev. Lett.* **94**, 192301 (2005).
- [15] See *e.g.* U. Heinz, P. Kolb, *Phys. Rev.* **C65**, 054909 (2000).
- [16] F. Retiere, M. Lisa, *Phys. Rev.* **C70**, 044907 (2004).
- [17] F. Antinori *et al.*, *J. Phys.* **G30**, 823 (2004).
- [18] H. Appelshäuser *et al.*, *Eur. Phys. J.* **C2**, 661 (1998).
- [19] M. Borysova *et al.*, *Phys. Rev.* **C73**, 024903 (2006).
- [20] C. Alt *et al.*, *Phys. Rev.* **C68**, 034903 (2003).
- [21] G. Stefanek (NA49 Collaboration), *Nucl. Phys.* **A774**, 499 (2006).
- [22] D. Teaney *et al.*, *Phys. Rev. Lett.* **86**, 4783 (2001).
- [23] See *e.g.* F. Becattini *et al.*, *Phys. Rev.* **C69**, 024905 (2004).
- [24] J. Cleymans, K. Redlich, *Phys. Rev. Lett.* **81**, 5284 (1998).
- [25] RQMD: F. Wang *et al.*, *Phys. Rev.* **C61**, 064904 (2000); UrQMD: H. Weber *et al.*, *Phys. Lett.* **B545**, 285 (2002).
- [26] J. Cleymans *et al.*, *Phys. Lett.* **B615**, 50 (2005).
- [27] M. Gorenstein, M. Gaździcki, K. Bugaev, *Phys. Lett.* **B567**, 175 (2003).
- [28] F. Hama *et al.*, *Acta Phys. Pol. B* **35**, 179 (2004).
- [29] T. Anticic *et al.*, *Phys. Rev.* **C70**, 034902 (2004).
- [30] St. Mrówczyński *et al.*, *Phys. Rev.* **C70**, 054906 (2004).
- [31] D. Adamova *et al.*, *Nucl. Phys.* **A727**, 97 (2003).

- [32] J. Adams *et al.*, *Phys. Rev.* **C71**, 064906 (2005).
- [33] M. Gorenstein *et al.*, *Phys. Lett.* **B585**, 237 (2004).
- [34] C. Roland (NA49 Collaboration), *J. Phys. G* **30**, S1381 (2004).
- [35] H. Appelshäuser *et al.*, *Phys. Lett.* **B459**, 679 (1999).
- [36] S. Das (STAR Collaboration), nucl-ex/0503023 (SQM2005 and SQM2006 contributions).
- [37] S. Jeon, V. Koch, *Phys. Rev. Lett.* **85**, 2076 (2000); M. Asakawa *et al.*, *Phys. Rev. Lett.* **85**, 2072 (2000).
- [38] C. Alt *et al.*, *Phys. Rev.* **C70**, 064903 (2004).
- [39] A. Bialas, *Phys. Lett.* **B532**, 249 (2002).
- [40] J. Zaranek, *Phys. Rev.* **C66**, 024905 (2002).
- [41] S. Bass *et al.*, *Phys. Rev. Lett.* **85**, 2689 (2000).
- [42] C. Alt *et al.*, *Phys. Rev.* **C71**, 034903 (2005).
- [43] J. Adams *et al.*, *Phys. Rev. Lett.* **90**, 172301 (2003).
- [44] A. Bialas, *Phys. Lett.* **B579**, 31 (2004).
- [45] Proceedings of the RIKEN BNL Workshop: Can we Discover the QCD Critical Point at RHIC?, BNL-75692-2006; <https://www.bnl.gov/riken/QCDRhic>.
- [46] J. Bartke, CERN-SPSC-2003-038(SPSC-EOI-01) and presentations at the Vilar Workshop (2004).
- [47] N. Antoniou *et al.*, CERN-SPSC-2006-001(SPSC-I-235).